Opto-Electronic Advances

Original Article

2020, Vol. 3, No. 3

DOI: 10.29026/oea.2020.190022

Ultrasensitive skin-like wearable optical sensors based on glass micro/nanofibers

Lei Zhang[1]*, Jing Pan[1], Zhang Zhang[1], Hao Wu[1], Ni Yao[1], Dawei Cai[1], Yingxin Xu[1], Jin Zhang[1], Guofei Sun[2], Liqiang Wang[1], Weidong Geng[2], Wenguang Jin[3], Wei Fang[1], Dawei Di[1,4] and Limin Tong[1]*

Electronic skin, a class of wearable electronic sensors that mimic the functionalities of human skin, has made remarkable success in applications including health monitoring, human-machine interaction and electronic-biological interfaces. While electronic skin continues to achieve higher sensitivity and faster response, its ultimate performance is fundamentally limited by the nature of low-frequency AC currents. Herein, highly sensitive skin-like wearable optical sensors are demonstrated by embedding glass micro/nanofibers (MNFs) in thin layers of polydimethylsiloxane (PDMS). Enabled by the transition from guided modes into radiation modes of the waveguiding MNFs upon external stimuli, the skin-like optical sensors show ultrahigh sensitivity (1870 kPa^{-1}), low detection limit (7 mPa) and fast response (10 μs) for pressure sensing, significantly exceeding the performance metrics of state-of-the-art electronic skins. Electromagnetic interference (EMI)-free detection of high-frequency vibrations, wrist pulse and human voice are realized. Moreover, a five-sensor optical data glove and a 2×2-MNF tactile sensor are demonstrated. These initial results pave the way toward a new category of optical devices ranging from ultrasensitive wearable sensors to optical skins.

Keywords: optical micro/nanofiber; pressure sensor; tactile sensor; wearable sensor

Zhang L, Pan J, Zhang Z, Wu H, Yao N et al. Ultrasensitive skin-like wearable optical sensors based on glass micro/nanofibers. *Opto-Electron Adv* **3**, 190022 (2020).

Introduction

Over the past decades, breakthroughs in flexible electronics and nanotechnology have enabled wearable electronic sensors[1,2] that respond to external stimuli via capacitive[3], resistive[4], piezoelectric[5], and triboelectric[6] effects. While microelectronic technologies continue to push wearable devices towards higher sensitivity, faster response, better robustness and denser integration[7–12], it may ultimately reach the limit imposed by the nature of low-frequency electromagnetic fields (i.e., AC currents). For example, response time is limited by parasitic effects and crosstalk in high-density electronic circuitries. In contrast, using photons instead of electrons as the signal carrier is an ideal strategy to circumvent these limitations[13], which has been shown in optical fiber sensors[14]. Conventional optical fibers, which are ~125 μm in diameter, are usually too thick and rigid to be made into a wearable device. Optical micro/nanofibers (MNFs), which are about 1 μm in diameter, are capable of guiding light with high flexibility[15]. Owing to their atomically-precise geometric uniformities, they offer waveguiding losses (e.g., <0.05 dB/cm[16]) much lower than any other optical waveguides of similar sizes, and mechanical strength (e.g., tensile strength>5 Gpa[17]) higher than spider silks (0.5–3.6 GPa[18]). Recently, MNFs have been at-

[1]State Key Laboratory of Modern Optical Instrumentation, College of Optical Science and Engineering, Zhejiang University, Hangzhou 310027, China; [2]College of Computer Science and Technology, Zhejiang University, Hangzhou 310027, China; [3]College of Information Science and Electronic Engineering, Zhejiang University, Hangzhou 310027, China; [4]Cavendish Laboratory, University of Cambridge, JJ Thomson Avenue, Cambridge CB3 0HE, United Kingdom.

*Correspondence: L Zhang, E-mail: zhang_lei@zju.edu.cn; L M Tong, E-mail: phytong@zju.edu.cn

Received: 21 June 2019; Accepted: 23 September 2019; Published: 20 March 2020

tracting increasing interest for optical trapping[19] and sensing applications, including biomolecular detection[20,21], refractive-index measurement[22–24], gas sensing[25,26], and microforce sensing[27,28]. Here we demonstrate a simple and general approach to wearable optical sensors by embedding glass MNFs in thin layers of polydimethylsiloxane (PDMS). Based on the transition from guided modes into radiation modes of the waveguiding MNFs upon external stimuli, the single-MNF optical sensors are demonstrated for pressure and vibration sensing with extraordinary high sensitivity and fast response. Moreover, a five-sensor optical data glove and 2×2-MNF tactile sensors are demonstrated for controlling the movement of a mechanical hand and detecting the exact location of a touch, respectively.

Results and discussion

In this work, highly uniform MNFs (Fig. 1(a)) are fabricated by taper drawing silica glass optical fibers (see the Supporting Information for details, Fig. S1), which are flexible in routing light at micrometer scale (Fig. 1(b)). However, the as-fabricated MNFs, with large fractional evanescent fields exposed to open air[29], are highly sensitive to environmental disturbance (e.g., direct physical pressure) or contamination (e.g., dust adsorption), which may lead to unpredictable variations of guided signals. To employ MNFs for wearable sensor applications, the guided optical fields must be well managed. Herein, we use a thin layer of PDMS, a highly flexible and biocompatible polymer with refractive index (n=1.40) slightly lower than that of silica (n=1.46), to enclose the MNF and isolate the evanescent fields, while maintaining high mechanical flexibility and low optical losses of the MNF (Fig. S2). The layer thickness, from 1 mm (e.g., 0.8 mm in Fig. 1(c)) to less than 100 μm (e.g., 80 μm in Fig. 1(d)), is sufficiently thick to contain the evanescent fields of the MNF typically extending several microns. Figs. 1(c) and 1(d) show typical MNF-embedded PDMS patches being bent in free space (Fig. 1(c)) or attached on human hand (Fig. 1(d)). Within a PDMS host film, the MNF can be made into various shapes (Fig. 1(e)), offering additional flexibility for stretching or bending. Meanwhile, at optical frequencies, the crosstalk between closely patterned MNFs can be minimized. Fig. 1(f) shows the arrangements of two MNFs with 3-μm spacing (top panel) and perpendicular crossing with direct contact (bottom panel), respectively. With green or red optical signals waveguided in individual MNFs, no crosstalk is observed.

The pressure response of a MNF-embedded PDMS patch adhered on a glass slide (Fig. 2(a)) is investigated by measuring the optical transmission through the MNF. As shown in Fig. 2(b), when the patch is slightly bent (e.g., at

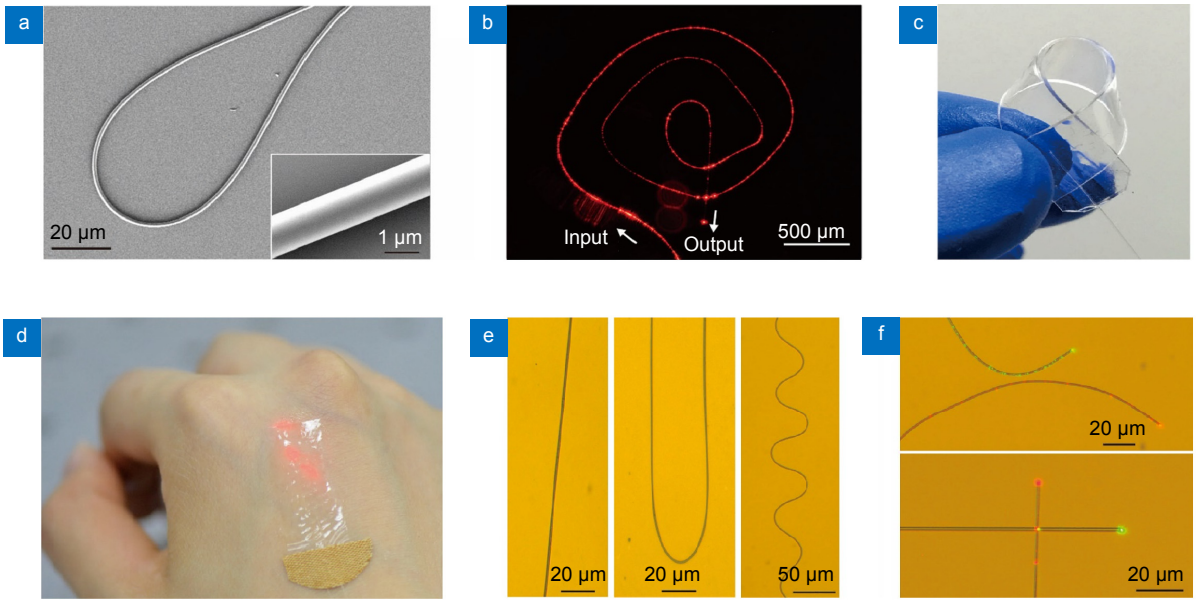

Fig. 1 | Fabrication and characterization of MNF-embedded PDMS patches. (**a**) SEM image of a 900-nm-diameter glass MNF with a bending radius of 30 μm. Inset: close-up image of the MNF showing smooth surface and uniform diameter. (**b**) Optical microscope image of a 1-μm-diameter glass MNF spiral guiding a 633-nm optical signal on a MgF_2 substrate. (**c**) Photograph of a bent MNF-embedded PDMS patch. (**d**) Photograph of a MNF-embedded PDMS patch attached on human hand. (**e**) Optical microscope images of three patches with straight (left), bent (middle), and wavy (right) MNFs, respectively. (**f**) Optical microscope images of two MNFs guiding 532- and 633-nm signals separately. The two MNFs are assembled into side-by-side (top) and perpendicular crossing structures (bottom), with no crosstalk observed.

a bending angle of 5°, induced by pressure), the well confined symmetric mode of a 1-μm-diameter MNF at the input port evolves into an asymmetric profile with clear optical leakage after propagating merely 100 μm, making it a skin-like wearable optical sensor (SLWOS) highly sensitive to micro-deformation. For example, upon a slight touch of a finger, light leakage from the PDMS patch is clearly observed (Fig. 2(c)).

Fig. 2(d) gives typical response of three 120-μm-thickness SLWOSs (with MNF diameters of 800 nm, 1.5 μm, and 2.8 μm, respectively) by laterally scanning a 10-kPa pressure perpendicular to the MNF. Using 790-nm probe light, the sensor starts to function from a lateral offset of about 700 μm (y=700 μm), with maxima at zero offset (y=0). Also, the thinner MNF gives higher sensitivity due to the larger fraction of evanescent fields (Fig. S3). Meanwhile, using a tungsten lamp as the probe light, we are able to obtain broadband spectral response in a single measurement. Fig. 2(e) shows broadband wavelength-dependent response to pressures from 2 to 10 kPa. With increasing wavelength, the output intensity of the MNF decreases and the sensitivity increases, as a result of the increasing fractional evanescent fields. The broadband wavelength-dependent response offers an opportunity for tuning the sensitivity and detection range in the same sensor using different wavelengths, and thus broadens the dynamic range without sacrificing sensitivity in a SLWOS (Fig. S4). In addition, by using purely

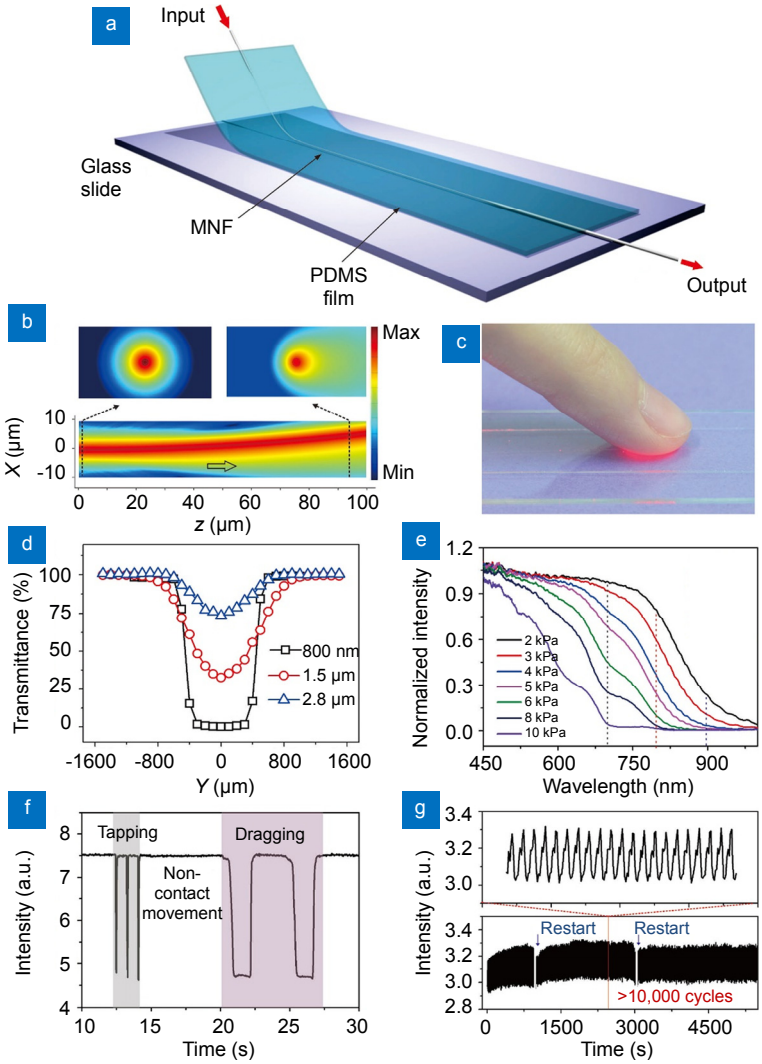

Fig. 2 | Characterization of substrate supported SLWOSs. (**a**) Schematic of testing a SLWOS on a glass slide. (**b**) Optical field intensity distributions of 900-nm-wavelength light guiding along a 1-μm-diameter glass MNF embedded in a 5°-bent SLWOS. (**c**) Photograph of light leaking out of a SLWOS upon a finger touch. (**d**) Lateral pressure response of a SLWOS with MNF diameters of 0.8, 1.5 and 2.8 μm, respectively. (**e**) Pressure response of a SLWOS with a wide spectral range. (**f**) Typical response of a SLWOS to finger movements of tapping, non-contact movement and dragging successively. (**g**) Long-term operational characteristics of a SLWOS measured by alternately applying/removing a 2-kPa pressure for more than 10,000 cycles.

optical effects, the SLWOS is completely EMI-free. Fig. 2(f) shows the response of a SLWOS to finger actions of tapping, non-contact movement and dragging successively (see Movie S1 in Supporting Information). Note that the action of "non-contact movement" means that the finger moves above the surface of the SLWOS, but not apply pressure on the SLWOS. The action of "dragging" indicates the finger moves on the surface of the SLWOS with contact and pressure. It is clear that "tapping" and "dragging" lead to obvious decrease of the transmittance, but "non-contact movement" does not result in any detectable change of transmittance. The result confirms that the human body, a grounded conducting medium, has no impacts on the SLWOS. The distinguishability of the three types of actions of the SLWOS circumvents the EMI issue in electronic devices (e.g., capacity-sensitive sensors[30]). Also, the water-proof SLWOS can be operated in a conductive liquid medium (see Movie S2 in Supporting Information). The long-term operational stability and excellent reliability of the SLWOS is verified by alternately applying/removing a 2-kPa pressure for more than 10,000 cycles (Fig. 2(g)).

To work more flexibly, the SLWOS should conform to non-flat surfaces or be operational in a suspended mode.

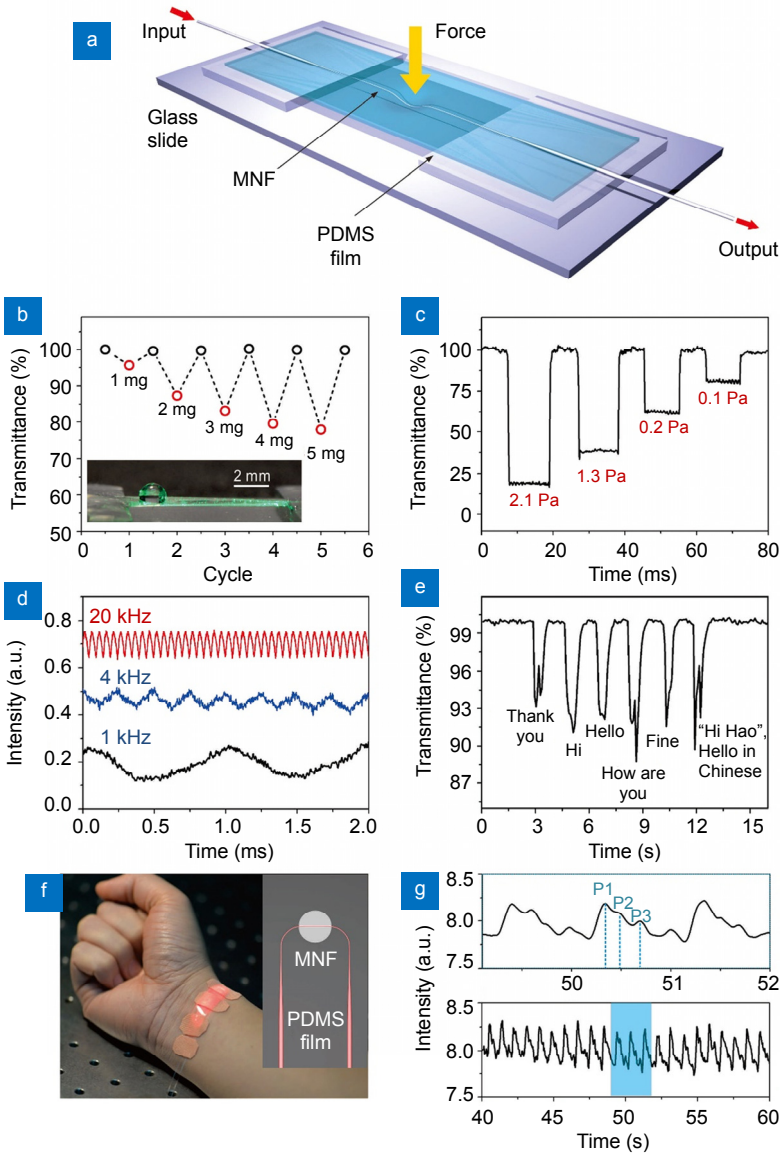

Fig. 3 | Characterization of suspended SLWOSs. (**a**) Schematic of testing suspended SLWOS. (**b**) Response of a suspended SLWOS to water droplets with different weights. The inset shows an optical micrograph of the SLWOS with a water droplet atop. (**c**) Response of a suspended SLWOS to pressure of 2.1, 1.3, 0.2 and 0.1 Pa, respectively. (**d**) Temporary response of a suspended SLWOS to forced oscillation frequencies of 1, 4 and 20 kHz, respectively. (**e**) Response of a suspended SLWOS to acoustic vibrations from human voice. (**f**) Photograph showing a SLWOS directly above the artery of the wrist. The inset shows a schematic of the SLWOS. (**g**) Measurement of wrist pulse under normal-condition (66 beats per minute).

Fig. 3(a) shows a schematic diagram of a suspended SLWOS that responds to external force with a micro pit. Under the same pressure, a suspended SLWOS allows higher degrees of deformation, offering better sensitivity than that attached on rigid surfaces (e.g., Fig. 2(a)). Fig. 3(b) shows the response of a suspended SLWOS (80-μm thickness, 980-nm MNF diameter), showing its ability to detect a water droplet down to 1 mg in weight that is too small to cause any observable deformation of the SLWOS (inset of Fig. 3(b)). To examine the detection limit of this type of devices, a calibrated stream of airflow is used to apply a small pressure (Figs. S5(a) and 5(b)) on a suspended SLWOS (50-μm thickness, 780-nm-diameter MNF). The clear response of the SLWOS to pressures down to 0.1 Pa with a high signal-to-noise ratio (Fig. 3(c)) corresponds to a detection limit of about 7 mPa. Moreover, with pressure lower than 0.2 Pa, the SLWOS offers a sensitivity of as high as 1870 kPa^{-1} (Fig. S5(c) and 5(d)), which is much more sensitive than that of high-performance electronic-skin sensors (e.g., 0.55–192 kPa^{-1})[31–33].

To investigate the temporary response, a SLWOS (80-μm thickness, 1.2-μm MNF diameter) is used to measure mechanical vibration (Fig. S6). The clear distinguishability up to 20 kHz (Fig. 3(d)), corresponding to a response time of ~10 μs, is more than three orders of magnitude faster than fast-response electronic-skin sensors (10-30 ms)[34–36]. In principle, without parasitic electrical effects, a SLWOS should be able to respond even more rapidly, when a higher-frequency vibration test platform is available. Not surprisingly, the SLWOS is highly sensitive to voice that propagates as acoustic waves in air (Fig. 3(e)), offering a possibility to resolve weak and rapid fluctuation of air pressure in real-time. Also, when being attached to a hand wrist (Fig. 3(f)), a SLWOS can readily read out wrist pulse with high resolution (Fig. 3(g)), the two distinguishable peaks (P1 and P3) and a late systolic augmentation shoulder (P2), agree very well with the noninvasive high-fidelity recording of the radial artery pressure wave[37].

Individual SLWOS can also be employed in multi-channel sensing. Fig. 4(a) shows a five-sensor optical data glove for monitoring the flexion and extension of the metacarpophalangeal (MCP) joints of individual fingers (see Movie S3 in Supporting Information), presenting a monotonic and approximately linear dependence of individual SLWOS output on the bending angle (Fig. 4(b)) with an angular resolution of better than 0.2° (Fig. 4(c)), which is much higher than that of the data gloves constructed from standard fiber-optic sensors (e.g., 1.8°)[38] and stretchable conductive fiber strain sensors (e.g., 1.5°)[39].

With negligible crosstalk (Fig. 1(f)), multiple MNFs can also be weaved inside a single SLWOS for spatially resolved 2-dimensional tactile sensing. Fig. 4(d) shows a SLWOS (200-μm-thick) embedded with perpendicularly

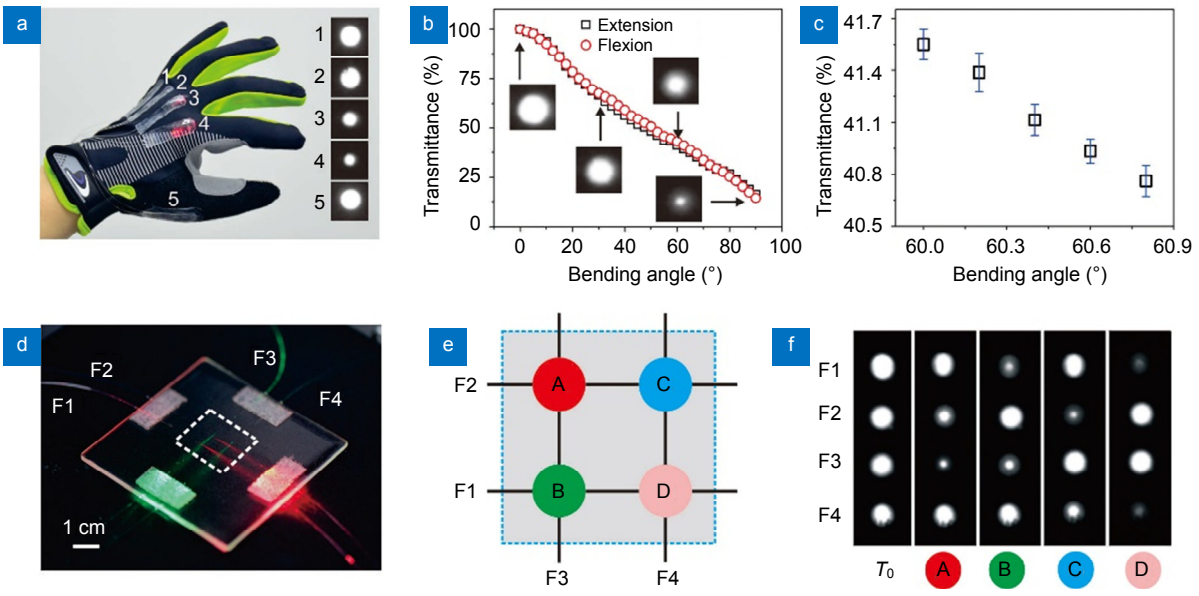

Fig. 4 | Optical data gloves and SLWOS with perpendicularly intersected 2×2 MNF arrays. (**a**) Photograph showing a five-sensor data glove integrated with 5 SLWOSs. (**b**) Bending-angle-dependent output of a typical SLWOS. (**c**) Close-up view of the SLWOS output within bending angles of 60.0°–60.8°. (**d**) Photograph showing a SLWOS consisted by a perpendicularly intersected 2×2 MNF array. (**e**) Schematic of the sensing areas for tactile sensing. (**f**) Logic outputs of a 4-input/output-port SLWOS.

intersected 2×2 MNF arrays (15-mm separation between neighboring MNFs). When pressure is applied on the net-joint areas from node A to node D successively (Fig. 4(e)), logic readouts can be obtained (see Fig. 4(f) and Table S1): with zero external pressure (T_0), the four outputs read high; when the pressure is exerted on a certain point (e.g., node A), the two channels that cross the point (e.g., channels F2 and F3 at node A) give low output due to pressure-induced losses, while the others remain to be high. For spatially denser pressure sensing, the logic functionality of SLWOS with smaller MNF separation (e.g., 3 mm) has also been realized (Fig. S7 and Table S2). Finally, it is worth mentioning that, the power of the probe light (coupled from an LED) in the above-mentioned SLWOS is about 400 nW, which can be further reduced through optimization, offering opportunities for ultralow-power operation.

Conclusions

We have demonstrated a new class of wearable optical sensors that greatly surpasses conventional wearable sensors in sensitivity, response time and EMI immunity. In principle, the sensitivity of the SLWOS can still be significantly improved when the refractive index of the host film approaches that of the MNF, and the response time is only limited by the mechanical properties of the hybrid MNF-PDMS structure. Meanwhile, the minimized optical crosstalk points toward the possibility of realizing multifunctional SLWOS based on high-density optical circuitries, and the simple hybrid structures allow excellent versatility and large-scale fabrication. Our results may pave the way towards future wearable optical devices for applications including human-machine interfaces, health monitoring and artificial intelligence.

References

1. Kim D H, Lu N S, Ma R, Kim Y S, Kim R H et al. Epidermal electronics. *Science* **333**, 838–843 (2011).
2. Hammock M L, Chortos A, Tee B C K, Tok J B H, Bao Z N. 25th anniversary article: the evolution of electronic skin (E-Skin): a brief history, design considerations, and recent progress. *Adv Mater* **25**, 5997–6038 (2013).
3. Mannsfeld S C B, Tee B C K, Stoltenberg R M, Chen C V H H, Barman S et al. Highly sensitive flexible pressure sensors with microstructured rubber dielectric layers. *Nat Mater* **9**, 859–864 (2010).
4. Jason N N, Ho M D, Cheng W J. Resistive electronic skin. *J Mater Chem C* **5**, 5845–5866 (2017).
5. Wang X D, Zhou J, Song J H, Liu J, Xu N S et al. Piezoelectric field effect transistor and nanoforce sensor based on a single ZnO nanowire. *Nano Lett* **6**, 2768–2772 (2006).
6. Fan F R, Lin L, Zhu G, Wu W Z, Zhang R et al. Transparent triboelectric nanogenerators and self-powered pressure sensors based on micropatterned plastic films. *Nano Lett* **12**, 3109–3114 (2012).
7. Kang D, Pikhitsa P V, Choi Y W, Lee C, Shin S S et al. Ultrasensitive mechanical crack-based sensor inspired by the spider sensory system. *Nature* **516**, 222–226 (2014).
8. Yin D, Feng J, Ma R, Liu Y F, Zhang Y L et al. Efficient and mechanically robust stretchable organic light-emitting devices by a laser-programmable buckling process. *Nat Commun* **7**, 11573 (2016).
9. Miyamoto A, Lee S, Cooray N F, Lee S, Mori M et al. Inflammation-free, gas-permeable, lightweight, stretchable on-skin electronics with nanomeshes. *Nat Nanotechnol* **12**, 907–913 (2017).
10. Takei K, Takahashi T, Ho J C, Ko H, Gillies A G et al. Nanowire active-matrix circuitry for low-voltage macroscale artificial skin. *Nat Mater* **9**, 821–826 (2010).
11. Larson C, Peele B, Li S, Robinson S, Totaro M et al. Highly stretchable electroluminescent skin for optical signaling and tactile sensing. *Science* **351**, 1071–1074 (2016).
12. Kim Y, Chortos A, Xu W T, Liu Y X, Oh J Y et al. A bioinspired flexible organic artificial afferent nerve. *Science* **360**, 998–1003 (2018).
13. Miller D A B. Rationale and challenges for optical interconnects to electronic chips. *Proc IEEE* **88**, 728–749 (2000).
14. Lee B. Review of the present status of optical fiber sensors. *Opt Fiber Technol* **9**, 57–79 (2003).
15. Tong L M, Gattass R R, Ashcom J B, He S L, Lou J Y et al. Subwavelength-diameter silica wires for low-loss optical wave guiding. *Nature* **426**, 816–819 (2003).
16. Nagai R, Aoki T. Ultra-low-loss tapered optical fibers with minimal lengths. *Opt Express* **22**, 28427–28436 (2014).
17. Brambilla G, Payne D N. The ultimate strength of glass silica nanowires. *Nano Lett* **9**, 831–835 (2019).
18. Rising A, Johansson J. Toward spinning artificial spider silk. *Nat Chem Biol* **11**, 309–315 (2015).
19. Daly M, Sergides M, Nic Chormaic S. Optical trapping and manipulation of micrometer and submicrometer particles. *Laser Photonics Rev* **9**, 309–329 (2015).
20. Sun D D, Guo T, Ran Y, Huang Y, Guan B O. *In-situ* DNA hybridization detection with a reflective microfiber grating biosensor. *Biosens Bioelectron* **61**, 541–546 (2014).
21. Liu T, Liang L L, Xiao P, Sun L P, Huang Y Y et al. A label-free cardiac biomarker immunosensor based on phase-shifted microfiber Bragg grating. *Biosens Bioelectron* **100**, 155–160 (2018).
22. Sumetsky M, Windeler R S, Dulashko Y, Fan X. Optical liquid ring resonator sensor. *Opt Express* **15**, 14376–14381 (2007).
23. Wang C, Jin W, Liao C R, Ma J, Jin W et al. Highly birefringent suspended-core photonic microcells for refractive-index sensing. *Appl Phys Lett* **105**, 061105 (2014).
24. Luo H P, Sun Q Z, Li X L, Yan Z J, Li Y P et al. Refractive index sensitivity characteristics near the dispersion turning point of the multimode microfiber-based Mach–Zehnder interferometer. *Opt Lett* **40**, 5042–5045 (2015).
25. Gu F X, Wu G Q, Zeng H P. Hybrid photon–plasmon Mach–Zehnder interferometers for highly sensitive hydrogen sensing. *Nanoscale* **7**, 924–929 (2015).
26. Wu Y, Yao B C, Yu C B, Rao Y J. Optical graphene gas sensors based on microfibers: a review. *Sensors* **18**, 941 (2018).
27. Chen Y, Yan S C, Zheng X, Xu F, Lu Y Q. A miniature reflective micro-force sensor based on a microfiber coupler. *Opt Express* **22**, 2443–2450 (2014).

28. Yang R, Yu Y S, Zhu C C, Xue Y, Chen C et al. PDMS-coated S-tapered fiber for highly sensitive measurements of transverse load and temperature. *IEEE Sens J* **15**, 3429–3435 (2015).
29. Tong L M, Lou J Y, Mazur E. Single-mode guiding properties of subwavelength-diameter silica and silicon wire waveguides. *Opt Express* **12**, 1025–1035 (2004).
30. Zhao X L, Hua Q L, Yu R M, Zhang Y, Pan C F. Flexible, stretchable and wearable multifunctional sensor array as artificial electronic skin for static and dynamic strain mapping. *Adv Electron Mater* **1**, 1500142 (2015).
31. Persano L, Dagdeviren C, Su Y W, Zhang Y H, Girardo S et al. High performance piezoelectric devices based on aligned arrays of nanofibers of poly(vinylidenefluoride-co-trifluoroethylene). *Nat Commun* **4**, 1633 (2013).
32. Park J, Lee Y, Hong J, Ha M, Jung Y D et al. Giant tunneling piezoresistance of composite elastomers with interlocked microdome arrays for ultrasensitive and multimodal electronic skins. *ACS Nano* **8**, 4689–4697 (2014).
33. Zang Y P, Zhang F J, Huang D Z, Gao X K, Di C A et al. Flexible suspended gate organic thin-film transistors for ultra-sensitive pressure detection. *Nat Commun* **6**, 6269 (2015).
34. Zhou J, Gu Y D, Fei P, Mai W J, Gao Y F et al. Flexible piezotronic strain sensor. *Nano Lett* **8**, 3035–3040 (2008).
35. Wang X W, Gu Y, Xiong Z P, Cui Z, Zhang T. Silk‐molded flexible, ultrasensitive, and highly stable electronic skin for monitoring human physiological signals. *Adv Mater* **26**, 1336–1342 (2014).
36. Shin S H, Ji S, Choi S, Pyo K H, Wan A B et al. Integrated arrays of air-dielectric graphene transistors as transparent active-matrix pressure sensors for wide pressure ranges. *Nat Commun* **8**, 14950 (2017).
37. Nichols W W. Clinical measurement of arterial stiffness obtained from noninvasive pressure waveforms. *Am J Hypertens* **18**, 3–10 (2005).
38. Fujiwara E, dos Santos M F M, Suzuki C K. Flexible optical fiber bending transducer for application in glove-based sensors. *IEEE Sens J*, **14**, 3631–3636 (2014).
39. Chen S, Lou Z, Chen D, Jiang K, Shen G Z. Polymer-enhanced highly stretchable conductive fiber strain sensor used for electronic data gloves. *Adv Mater Technol* 1, 1600136 (2016).

Acknowledgements

This work was supported by the National Key Research and Development Program of China (2016YFB1001300), the National Natural Science Foundation of China (No. 11527901) and the Fundamental Research Funds for the Central Universities.

Author contributions

L. Z. and L. T. conceived the project idea and designed the experiments. L. Z., J. P., Z. Z., N. Y., D. C., and Y. X. carried out the experiments and collected the data. J. Z., L. W., G. S., W. G. contributed to LED, CCD, and the software of the 5-sensor data glove. H. W. contributed to bending loss simulations. L. Z., L. T., and D. D. analyzed all the data and cowrote the paper. All authors discussed the results and commented on the manuscript.

Competing interests

The authors declare no competing financial interests.

Supplementary information

Supplementary information for this paper is available at https://doi.org/10.29026/oea.2020.190022